JOURNAL OF SPACECRAFT AND ROCKETS
Vol. 37, No. 4, July–August 2000

# Application of Multidisciplinary Design Optimization Techniques to Distributed Satellite Systems

Cyrus D. Jilla,* David W. Miller,† and Raymond J. Sedwick‡
*Massachusetts Institute of Technology, Cambridge, Massachusetts 02139*

**Four separate multidisciplinary design optimization techniques have been investigated for their applicability to the rapid conceptual design of distributed satellite systems. The four multidisciplinary design optimization techniques tested were Taguchi's method, simulated annealing, a pseudogradient search, and single-variable-axis exploration. Each multidisciplinary design optimization technique was applied to the problem of developing a systems architecture that minimizes a multicriterion metric (cost per image) for the NASA Origins Terrestrial Planet Finder mission. The best solution obtained from each technique after evaluating only 7.3–7.8% of all possible solutions was compared with the true optimal solution obtained from complete enumeration. It was found that although the simulated annealing, pseudogradient search, and single-variable-axis exploration algorithms all found the true optimal solution at least once over 10 trials, simulated annealing did so with the greatest degree of confidence statistically. Although Taguchi's method was unable to find the optimal solution, this method did provide useful ancillary information that the other techniques did not provide.**

## Nomenclature

$A$ = state coefficient matrix
$B$ = interferometer baseline, m
$C_{\text{bus}}$ = spacecraft bus cost, $M
$C_{\text{launch}}$ = launch cost, $M
$C_{\text{operations}}$ = life-cycle operations cost, $M
$C_{\text{payload}}$ = spacecraft payload cost, $M
$D$ = aperture diameter
$E$ = system energy
$f$ = failure rate
$I$ = imaging rate, images/day
$I_d$ = deep spectroscopy imaging rate, images/day
$I_m$ = medium spectroscopy imaging rate, images/day
$I_s$ = survey image rate, images/day
$L$ = distance between aperture and array center, m
$m_{\gamma_x}$ = main effect of design variable $\gamma$ at setting $x$
$P$ = state probability vector
$\dot{P}$ = time rate of change of the state probability vector
$Q_{\text{dark}}$ = detector noise, photons$^2$/day
$Q_{\text{EZ}}$ = exozodiacal signal, photons$^2$/day
$Q_{\text{flat}}$ = background noise, photons$^2$/day
$Q_{\text{LZ}}$ = local zodiacal signal, photons$^2$/day
$Q_{\text{leak}}$ = leakage signal, photons$^2$/day
$Q_{\text{planet}}$ = planet signal, photons/day
$r$ = angular separation of the source from the center of the interferometer's fringe pattern, rad
$T$ = system temperature
$T_o$ = imaging overhead time, days
$y$ = year of the mission
$\Gamma$ = design vector
$\gamma_1$ = heliocentric orbital altitude, AU
$\gamma_2$ = collector connectivity/geometry
$\gamma_3$ = number of collector apertures
$\gamma_4$ = collector aperture diameter, m
$\delta$ = clock angle
$\eta$ = single-to-noise ratio of a Taguchi experiment
$\theta$ = azimuthal angle of the source from the first interferometric arm, rad
$\theta_r$ = angular resolution, milliarc sec
$\lambda$ = observation wavelength, m
$\mu$ = mean
$\nu$ = variance
$\sigma$ = standard deviation
$\tau$ = image integration time, days
$\Phi$ = total cost, $M
$\phi$ = independent phase shift
$\Psi$ = number of images
$\Omega$ = null depth

Received 5 November 1999; revision received 5 March 2000; accepted for publication 17 March 2000. 

*Graduate Research Assistant, Department of Aeronautics and Astronautics. Student Member AIAA.
†Professor, Department of Aeronautics and Astronautics. Member AIAA.
‡Research Scientist, Department of Aeronautics and Astronautics. Member AIAA.

## Introduction

OPTIMIZATION is defined as the process of achieving the most favorable system condition on the basis of a metric. Within the past 50 years, different optimization techniques have been applied to numerous complex problems, ranging from the design of airline flight networks that maximize revenues[1] under scheduling constraints[2] to the allocation of assets in portfolios on Wall Street under financial, regulatory, and risk constraints.[3] This paper explores the potential of four separate multidisciplinary design optimization (MDO) techniques—Taguchi's method, simulated annealing, a pseudogradient search, and the single-axis exploration algorithm—in the design of distributed satellite systems (DSSs).

Currently, the conceptual design of space systems tends to be unstructured, with designers often pursuing a single concept or modifying an existing idea rather than generating new alternatives. With such an approach, there is no guarantee that a systems-level focus will be taken, and often the final design architecture chosen achieves only feasibility instead of optimality.[4] Systems-level trades are often delayed until after a point design has been selected because of the perceived time and effort required for conducting a credible analysis.[5] Further complicating matters is the transition in the aerospace industry over the past decade from maximizing performance under technology constraints to minimizing cost with performance requirements.[4] If the system trade space is not properly explored and thus does not converge on an efficient or even an optimal solution during the conceptual design phase, the life-cycle cost of the system can greatly increase as modifications are required for properly integrating and operating the system during the latter stages of the design process, when design changes become much more expensive to implement.[6]

The pitfalls in not following a structured process during conceptual design hold especially true for DSSs, which tend to be among the most complex and expensive space systems. A DSS

is defined as a system of multiple satellites designed to work in a coordinated fashion to perform a mission.[7] Examples include the global positioning system (GPS) for navigation, the recently deployed low-Earth-orbit global mobile telephony constellations, and proposed separated spacecraft interferometers for astronomy. The advantages of distributed systems over traditional single satellite deployments—including potential improvements in performance, cost, and survivability—have led to an increase in the number of space missions that are considering distributed approaches.

DSSs are among the most challenging conceptual design problems as such complex systems often contain a large number of nonlinear, highly coupled variables. Take the example of a formation-flying separated spacecraft interferometer designed to image extrasolar planets. Both the total number of spacecraft in the array and the orbit of the interferometer drive the selection of the launch vehicle, which can be a dominant contributor to the system cost. The total number of spacecraft in the array also directly determines the operations complexity (nonlinear effect on operations cost) and indirectly determines the imaging rate (scales with the total collecting area). Likewise, the orbit also affects the imaging rate by determining the amount of local zodiacal dust (imaging noise source) the interferometer must peer through, and so forth. As in all DSSs, countless trades exist between system performance, system cost, and each of the design parameters, both individually and in combination with other design parameters. Thus a tool is needed to enable a greater search of the trade space and to explore design options that might not otherwise be considered.

Optimization is one such tool. In its pure mathematical definition, optimization refers to finding the absolute best solution to a problem. This definition will not be used here, however. Rather, the engineering interpretation of optimization will be referred to as the process of finding good solutions to the design problem. Because DSS design problems tend to be combinatorial in nature, with discrete variables that have nonlinear relationships, classical optimization techniques that require continuously differentiable convex functions, such as the simplex method, cannot be used. Rather, algorithms that can handle discrete, nonlinear problems with multiple criteria objective functions and constraints are required. This class of algorithms falls under a field known as MDO.[8] Different MDO techniques have recently been investigated for application to the design of interplanetary spacecraft,[9] small satellites,[5] and the Earth Observing System[10] with varying degrees of success.

The objective of this work is to explore and demonstrate the application of four separate MDO techniques—Taguchi's method, simulated annealing, a pseudogradient search, and single-axis exploration—to the design of a DSS. Given many different potential design configurations that fulfill system operational requirements with different degrees of performance and cost, the goal is to find a design architecture that minimizes the cost per function while meeting all requirements. Each technique is applied to the design of a real DSS to measure and compare how well the different methods perform. Once again, it should be stressed that none of the techniques explored here are guaranteed to find global optima but should find good solutions. The goal in applying MDO techniques to the design of DSSs is not to fully automate the design process and remove humans from the design loop, but rather to facilitate the conceptual design process, considered by many mission leaders to be the most important stage of design, often defining the line between success and failure.[11] MDO may be able to achieve this improvement of the conceptual design process by enabling a greater, more efficient exploration of the system trade space to find robust and perhaps even counterintuitive design architectures meriting further detailed analysis that might not otherwise be considered.

The remainder of this paper documents how the above objective was achieved. First, the DSS design case study that each of the four MDO techniques was applied to is introduced. Next, each of the four MDO techniques is summarized, including the origin of the technique, a summary explanation of how the technique works, and an outline of how the technique was tailored for application to the case study. Finally, the results of the case study are presented and compared, followed by the conclusions that may be drawn from an analysis of the results.

## DSS Application Test Study

To test and compare the effectiveness of the four chosen MDO techniques, they were each applied to the same DSS design problem—to find an architecture for NASA's Terrestrial Planet Finder (TPF) mission that maximizes the total number of images taken by the telescope while minimizing life-cycle cost.

The TPF is one in a series of missions as part of NASA's Origins Program, whose goal is to answer fundamental questions regarding the origin of life in the universe. Specifically, TPF will be the first spacecraft to directly detect the existence of Earth-like planets around neighboring stars.[12] Using the principles of nulling interferometry, TPF will suppress the light from the parent star by a factor of $10^6$ while maintaining good transmissivity in the parent star's habitable zone between 0.5 and 3 AU. Once identified, the TPF will carry out spectroscopic observations of these extrasolar planets to search for the chemical compounds that are capable of supporting life.[13]

The TPF mission is currently in the conceptual design phase, and several widely varying design architectures ranging from structurally connected to tethered to separated spacecraft arrays have been proposed. For the purpose of this case study, four design parameters are isolated as the key independent variables in the design problem—heliocentric orbital altitude ($\gamma_1$), collector connectivity/geometry ($\gamma_2$), number of collector apertures ($\gamma_3$), and the diameter of each collector aperture ($\gamma_4$). Together, these four parameters make up the TPF design vector $\Gamma$:

$$\Gamma = [\gamma_1 \quad \gamma_2 \quad \gamma_3 \quad \gamma_4] \tag{1}$$

Table 1 lists the range of discrete values considered for each design variable $\gamma$ in this case study. Each design vector defines a unique TPF mission architecture. The design vector was kept small to allow for the use of complete enumeration to verify the global minimum. With every possible combination of the variables in Table 1 taken into account, the trade space of this study contains 640 different design vectors or 640 unique TPF mission architectures. This set of architectures is defined as the full-factorial trade space.

A cost per function (CPF) metric will be used to evaluate the strength of each proposed TPF design architecture. For this mission, the CPF is defined as the cost per image (CPI). The objective for each of the MDO techniques is to find the TPF architecture that minimizes the CPI. The only constraints on the problem are those on the capability isolation (ability of the system to isolate and distinguish information signals from different noise sources within the field of view) and integrity (quality of the information passing through the network) requirements and the allowable values for each variable in the design vector. Other constraints, such as the maximum allowable program budget, have been omitted for the sake of simplicity in implementing the MDO algorithms. The TPF design optimization problem may now be represented mathematically as

$$\begin{aligned}
&\text{Objective:} && \min \frac{\sum_{y=1}^{5} \Phi_y(\Gamma)}{\sum_{y=1}^{5} \Psi_y(\Gamma)} \\
&\text{Constraints:} && \text{Subject to} \\
&\quad \text{Isolation} && \theta_r \geq 20 \text{ milliarc sec} \\
&\quad && \Omega \leq 10^{-6} \\
&\text{Integrity} && \\
&\quad \text{Surveying} && \text{SNR} \geq 5 \\
&\quad \text{Medium spectroscopy} && \text{SNR} \geq 10 \\
&\quad \text{Deep spectroscopy} && \text{SNR} \geq 25
\end{aligned} \tag{2}$$

**Table 1 The TPF design vector[a]**

| $\Gamma$ | Variable | Allowable values |
|---|---|---|
| $\gamma_1$ | Heliocentric orbital altitude, AU | 1.0, 1.5, 2.0, 2.5, 3.0, 3.5, 4.0, 4.5, 5.0, 5.5 |
| $\gamma_2$ | Collector connectivity/geometry | SCI-1D, SCI-2D, SSI-1D, SSI-2D |
| $\gamma_3$ | Numbers of collector apertures | 4, 6, 8, 10 |
| $\gamma_4$ | Diameter of collector apertures, m | 1, 2, 3, 4 |

[a]SCI, structurally connected interferometer; SSI, separated spacecraft interferometer; 1D, one-dimensional array; and 2D, two-dimensional array.

where $\Psi$ is the number of images (surveys + medium spectroscopies + deep spectroscopies) and SNR is the signal-to-noise ratio (photon count received from the planet over the photon count received from all noise sources).

The total life-cycle cost $\Phi$ in the objective function of representation (2) is obtained by summation of costs from both the design and operations phases of the TPF mission:

$$\sum_{y=1}^{5} \Phi_y = C_{\text{payload}} + C_{\text{bus}} + C_{\text{launch}} + C_{\text{operations}} \tag{3}$$

Both payload and spacecraft bus costs were computed with cost-estimation relationships from the U.S. Air Force Unmanned Spacecraft Cost Model.[14] Launch costs were obtained from published data,[15] and operations costs are a function of system complexity.[16]

System capability is a measure of the imaging rate of a TPF architecture. The minimum integration time required for observing a planet is

$$\tau = \left[\text{SNR}\sqrt{(Q_{\text{leak}} + Q_{\text{LZ}} + Q_{\text{EZ}} + Q_{\text{dark}} + Q_{\text{planet}} + Q_{\text{flat}})} \;/\; Q_{\text{planet}}\right]^2 \tag{4}$$

where $Q_{\text{planet}}$ is the planet signal modulated by the fringe pattern as the interferometer rotates around the line of sight to the star. The image rate $I$ is the inverse of the sum of the integration time $\tau$ and overhead time $T_o$, where overhead includes the time allotted for interferometer slewing, aperture configuration, array rotation, and mission operations inefficiency:

$$I = (\tau + T_o)^{-1} \tag{5}$$

Note that each TPF mission architecture will have three separate imaging rates as the required SNR for surveys, medium spectroscopies, and deep spectroscopies varies from 5 to 25.

Mission performance $\Psi$, in the objective function of Eq. (2), measures the total number of images the system obtains over 5 years, taking into account the degradation in system capability as partial failures occur over time. An example of system degradation would be the decrease in imaging rate that would result from the failure of one or more collector apertures in the interferometer. Markov reliability modeling techniques are used to determine both the probability that the system will continue to function over a given amount of time and the likelihood with which the system will function in different partially failed states throughout the mission.[16,17] From the Markov model, a system of differential equations is developed, as shown in Eq. (6):

$$\dot{P} = AP \tag{6}$$

where $A$ is the state coefficient matrix that comprises component failure rates.

Take the example of an eight-aperture TPF architecture. To apply a Markov modeling methodology, the states of the system must be time dependent, sequential, and mutually exclusive. If the system satisfies these requirements, then a set of differential equations can be written to model the evolution of the system by taking advantage of the Markov property, which states that, given full knowledge of the current state of the system, one can predict all future states by integrating a set of differential equations, irrespective of the past states

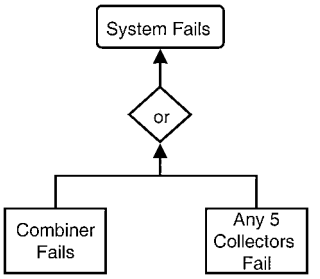


**Fig. 1 Aggregated fault tree for an eight-collector TPF architecture.**

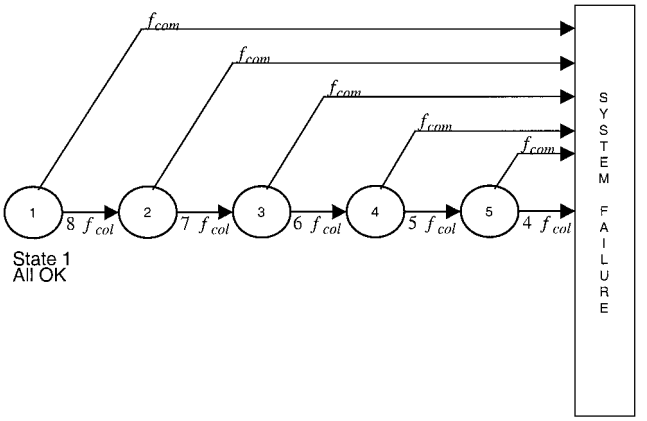


**Fig. 2 Aggregated Markov model state diagram for the eight-collector TPF architecture.**

of the system.[18] The first step in developing the Markov model for the eight-aperture TPF architecture is to develop a fault tree illustrating all the possible different failure modes (Fig. 1). The minimum functionality required for a nulling interferometer is one combiner and four collector apertures. Thus the eight-collector aperture TPF architecture fails when the combiner fails or when any five collectors fail. The system will still function when one to four collector apertures fail, but at a reduced capability (i.e., reduced imaging rate).

From the fault tree, a Markov model state diagram illustrating each possible state of the system may be created for each architecture. Figure 2 illustrates the Markov model for the eight-collector aperture architecture. This model contains five possible functioning states, all of which require a functional combiner: state 1, all eight collectors are working; state 2, seven of the eight collectors are working; state 3, six of the eight collectors are working; state 4, five of the eight collectors are working; and state 5, four of the eight collectors are working. Otherwise, the system is in a state of failure as the nulling (isolation) requirement can no longer be met.

From the Markov model state diagram, a system of differential equations can be written to determine the probability of the system being in any given state at any given time. This is done by representing each possible state of the system in the Markov model as a node in a network. To determine the differential equation for a particular state, the flow into and out of the node representing that state is balanced. The eight-collector TPF architecture requires a set of five partially coupled linear first-order differential equations to model the system:

$$\begin{bmatrix} \dot{P}_1 \\ \dot{P}_2 \\ \dot{P}_3 \\ \dot{P}_4 \\ \dot{P}_5 \end{bmatrix} = \begin{bmatrix} -(f_{\text{com}} + 8f_{\text{col}}) & 0 & 0 & 0 & 0 \\ 8f_{\text{col}} & -(f_{\text{com}} + 7f_{\text{col}}) & 0 & 0 & 0 \\ 0 & 7f_{\text{col}} & -(f_{\text{com}} + 6f_{\text{col}}) & 0 & 0 \\ 0 & 0 & 6f_{\text{col}} & -(f_{\text{com}} + 5f_{\text{col}}) & 0 \\ 0 & 0 & 0 & 5f_{\text{col}} & -(f_{\text{com}} + 4f_{\text{col}}) \end{bmatrix} \begin{bmatrix} P_1 \\ P_2 \\ P_3 \\ P_4 \\ P_5 \end{bmatrix} \tag{7}$$

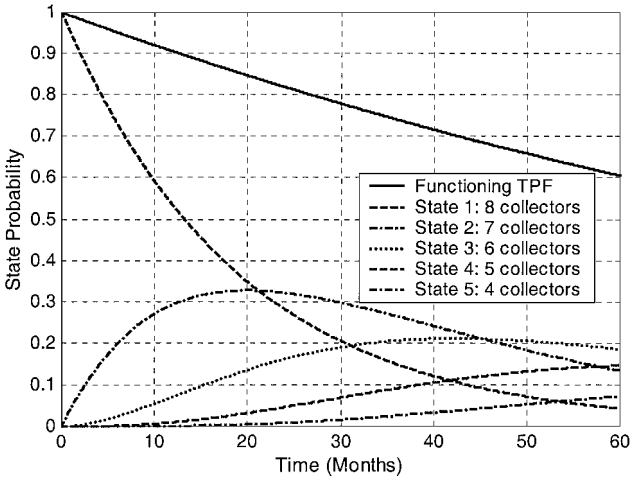


**Fig. 3 Markov model results for the eight-collector TPF architecture ($f_{com} = 5.5 \times 10^{-3}$ month$^{-1}$, $f_{col} = 8.3 \times 10^{-3}$ month$^{-1}$).**

Knowledge of the failure rates for the combiner ($f_{com}$) and collector ($f_{col}$) are required for solving for the state probabilities. The system's initial conditions are also required for the solution. In every case, the initial conditions (i.e., at $t = 0$ in the beginning of the operational mission) are a 100% probability of being in state one and a 0% probability of being in all successive states.

The plot in Fig. 3 illustrates the results for the eight-collector example. The Markov model gives the exact probability of being in any of the five operational states as a function of time through the 5-year (60-month) TPF mission. Each of these five operational states will have a different survey, medium spectroscopy, and deep spectroscopy imaging rate. The Markov models for architectures with 4–10 collectors were implemented in the same manner.

The solution to this system of differential equations [Eqs. (7)] determines the probability of the system being in any given state at a particular time. Coupling the outputs of the reliability model with the outputs of the capability model yields the total performance (total number of images $\Psi$) of the system. The coupling equation is

$$\begin{aligned}\sum_{y=1}^{5} \Psi_y = &\int_{74}^{256} \sum_{i=1}^{n} I_{si} P_i(t)\,dt + \int_{257}^{313} \sum_{i=1}^{n} I_{mi} P_i(t)\,dt + \int_{314}^{365} \sum_{i=1}^{n} I_{di} P_i(t)\,dt \\ &+ \int_{366}^{547} \sum_{i=1}^{n} I_{si} P_i(t)\,dt + \int_{548}^{658} \sum_{i=1}^{n} I_{mi} P_i(t)\,dt + \int_{659}^{730} \sum_{i=1}^{n} I_{di} P_i(t)\,dt \\ &+ \int_{731}^{804} \sum_{i=1}^{n} I_{si} P_i(t)\,dt + \int_{805}^{1004} \sum_{i=1}^{n} I_{mi} P_i(t)\,dt + \int_{1005}^{1095} \sum_{i=1}^{n} I_{di} P_i(t)\,dt \\ &+ \int_{1096}^{1132} \sum_{i=1}^{n} I_{si} P_i(t)\,dt + \int_{1133}^{1333} \sum_{i=1}^{n} I_{mi} P_i(t)\,dt + \int_{1334}^{1460} \sum_{i=1}^{n} I_{di} P_i(t)\,dt \\ &+ \int_{1461}^{1498} \sum_{i=1}^{n} I_{si} P_i(t)\,dt + \int_{1499}^{1680} \sum_{i=1}^{n} I_{mi} P_i(t)\,dt + \int_{1681}^{1825} \sum_{i=1}^{n} I_{di} P_i(t)\,dt \end{aligned} \tag{8}$$

where the limits of integration denote time steps of one day, $i$ is an index indicating a particular operational state, $n$ is the total number of operational states ($n = 5$ for the eight-collector aperture example), and $P$ is the probability of being in any state $i$ as a function of time $t$ [from Eq. (6)]. The imaging mode determines the SNR needed [Eq. (2)] to obtain the desired information on the target. This required SNR in turn determines the required integration time [Eq. (4)] and thus the imaging rate [Eq. (5)] in a particular mode. For example, the required SNR for a survey, in which the purpose is to determine whether a planet exists in the habitable zone around the target star, is only 5. The medium spectroscopy imaging mode searches for spectral lines (carbon dioxide and water) indicative of a planetary atmosphere and requires a SNR of 10. Deep spectroscopy searches for spectral lines (ozone and methane) that might signify the presence of a habitable environment or even the existence of life itself and requires a SNR of 25 (Ref. 13). Accordingly, surveys require the shortest integration time, and thus the survey-mode imaging rate $I_s$ is greater than $I_m$, and $I_m$ is greater than $I_d$. The limits of integration in Eq. (8) are based on a sample 5-year TPF mission profile.[13] The total system performance is obtained by the summation of 15 separate utility functions, in which each row in Eq. (8) denotes a separate year in the 5-year mission and each column denotes a different mission task (surveying, medium spectroscopy, and deep spectroscopy).

Finally, to determine whether or not the isolation constraints in Eq. (2) are met, the angular resolution and null depth must be computed for the desired TPF mission architecture. An interferometer's angular resolution $\theta_r$ is

$$\theta_r = \lambda / B \tag{9}$$

The nulling interference pattern communicated as the transmissivity function is given by

$$\Theta = \left| \sum_{k=1}^{N} D_k \exp\left( j2\pi \left( \frac{L_k r}{\lambda} \right) \cos(\delta_k - \theta) \right) \exp(j\phi_k) \right|^2 \tag{10}$$

where $D_k$ is the diameter of aperture $k$, $L_k$ is the distance between aperture $k$ and the center of the array, $\delta_k$ is clock angle of aperture $k$ measured from a given aperture, $\phi_k$ is the independent phase shift introduced to beam $k$, and $N$ is the number of apertures in the array.

To evaluate a potential TPF mission architecture on the basis of the objective function and constraints in Eq. (2) by use of the relationships in Eqs. (3–10), the design vector is entered into the TPF Mission Analysis Software (TMAS). TMAS is a MATLAB® program that captures the pertinent physics of the TPF mission and enables trade studies of different TPF architectures[19] with the Generalized Information Network Analysis (GINA) systems engineering methodology.[20]

Figure 4 illustrates the structure of the TMAS. The input that changes between each run of the program is the TPF design vector $\Gamma$. The constants vector contains values for all of the system variables that remain the same independent of the design vector. Examples of variables in the constants vector include the mission design life, the bandwidth for optical control, and the bending stiffness of the truss elements. The inputs from both the design and the constants vectors then feed into the six TMAS macromodules, each of which contains multiple submodules. First, the Environment

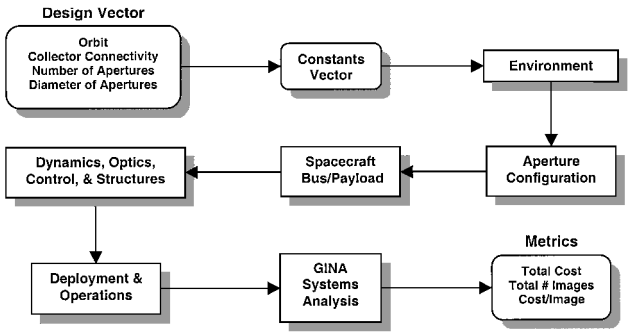


**Fig. 4 TMAS structure with six macromodules.**

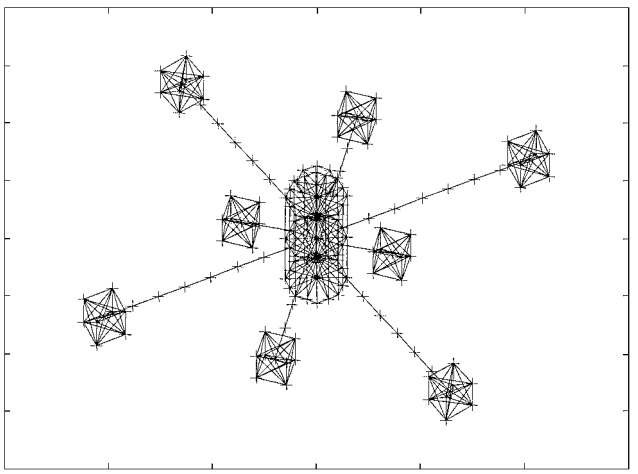

**Fig. 5 Finite element model for a TPF mission architecture with a design vector Γ = (4AU SCI-2D 8ap. 2m).**

macromodule computes properties such as solar flux and gravity gradient local to the selected TPF orbit. Next, the Aperture Configuration macromodule determines the optimal collector aperture geometry that satisfies both the nulling requirements and the architecture constraints. The Spacecraft Payload and Bus macromodule then designs and sizes all of the spacecraft. This information feeds into the Dynamics, Optics, Control, & Structures macromodule, which creates a finite-element model of the spacecraft (Fig. 5), designs an optical control system, and performs a disturbance analysis to ensure that optical path delay (OPD) tolerances are met. Next, the Deployment and Operations macromodule computes the orbital transfer parameters, selects a launch vehicle, assesses operations complexity, and estimates operations cost. Finally, the GINA Systems Analysis macromodule determines the system's ideal imaging rate in each operational mode, estimates the total number of images obtained over the mission design life, taking into account mission inefficiencies and spacecraft failures, and calculates the life-cycle cost.[16] In the end, the TMAS outputs a wide array of information to be used by the designer to assess the TPF design architecture, including the CPI metric to be minimized in the case study.

## Overview of MDO Techniques

DSS designs are discrete, nonlinear combinatorial problems: each design variable can take on only a set number of unique values. For this reason, continuous linear techniques such as the simplex method cannot be used. For this study, the chosen optimization methods are Taguchi's method, simulated annealing, pseudogradient search, and the single-axis exploration algorithm. The following subsections provide an overview of each technique, including the origin of the technique, a summary explanation of how the algorithm works, and the specifics of how the optimization technique was applied to the TPF design problem.

### Taguchi Methods

Beginning in the late 1970s, Genichi Taguchi of Japan created a framework that uses experimental design to improve the quality control of manufacturing processes.[21] Orthogonal arrays are used to define a set of experiments with different combinations of design variable settings. In an orthogonal test matrix, each value of each design variable is tested an equal number of times, and each of these values is tested with every value of all other design variables an equal number of times.[22] Although Taguchi methods have been used to improve the quality of manufacturing designs for many years now, these methods have only recently been considered for application to the design of aerospace systems. For example, Taguchi analysis has been used by engineers at the NASA Langley Research Center to create a Pareto-optimal design curve for a tetrahedral space truss platform by evaluating only 31 of the possible 19,683 truss designs.[23]

The size of the orthogonal design experiment matrix is a function of the total number of design variables and the number of different values each design variable may assume. Each row in this matrix represents a single experiment with a unique combination of design variable settings. The result of each experiment is converted into a parameter that Taguchi defines as the SNR, which combines the loss effects attributable to both missing a target and having too large a variation about that target.[21] It should be noted that this SNR is different from the SNR represented in Eq. (2). In the case in which the goal is to minimize the output of the metric of interest in each experiment, the SNR is defined as

$$\mathrm{SNR} = -10\log_{10}\left(\frac{1}{N}\sum z^2\right) \tag{11}$$

where $N$ is the total number of samples taken during an experiment and $z$ is the metric output of each sample of that particular experiment.[24]

After the experiments for every row in the orthogonal matrix have been completed and converted to SNRs the balanced mean $m$ for all of the experiments $n$ is calculated:

$$m = \frac{1}{n}\sum_{i=1}^{n}\eta_i \tag{12}$$

where $\eta$ is the SNR of each experiment $i$. Next, the main effect $(m_{\gamma_x})$ of each design variable $\gamma$ at a particular setting $x$ is computed:

$$m_{\gamma_x} = \frac{1}{n_{\gamma_x}}\sum_{i=1}^{n_{\gamma_x}}\eta_i \tag{13}$$

The most probable optimal design is then found by choosing the setting for each design variable that leads to the largest SNR. Finally, the performance $\eta_{\mathrm{opt}}$ of the proposed optimal design may be predicted:

$$\eta_{\mathrm{opt}} = m + \sum_{\gamma_i=1}^{d}\left(m_{\gamma_{ix}} - m\right) \tag{14}$$

where $d$ represents the total number of design variables in the experiment and $x$ denotes the proposed optimal setting for each design variable. If desired, additional computations may be made to assess the relative importance of each element of the design vector as well as the robustness of the final design.

For the TPF case study, a 48 × 4 orthogonal test matrix was required for properly conducting the Taguchi analysis, given the nature of the TPF design vector. Note that this required the use of two heliocentric orbital radii (6 and 6.5 AU) that were not in the original feasible space of the design vector. In the Taguchi analysis, however, their presence is required to ensure the statistical independence of the three other design vector elements. Because the "experiments" are computer simulations rather than actual physical experiments, the value of $N$ in Eq. (11) is 1. Table 2 illustrates the orthogonal test matrix for the TPF case study.

**Table 2 Orthogonal test matrix for the TPF case study**

| Case | Orbit, AU | Architecture | Number of apertures | Aperture diameter, m |
|---|---|---|---|---|
| 1 | 1 | SCI-1D | 4 | 1 |
| 2 | 1 | SCI-2D | 6 | 2 |
| 3 | 1 | SSI-1D | 8 | 3 |
| 4 | 1 | SSI-2D | 10 | 4 |
| 5 | 1.5 | SCI-1D | 6 | 3 |
| 6 | 1.5 | SCI-2D | 4 | 4 |
| 7 | 1.5 | SSI-1D | 10 | 1 |
| 8 | 1.5 | SSI-2D | 8 | 2 |
| 9 | 2 | SCI-1D | 8 | 4 |
| 10 | 2 | SCI-2D | 10 | 3 |
| 11 | 2 | SSI-1D | 4 | 2 |
| 12 | 2 | SSI-2D | 6 | 1 |
| 13 | 2.5 | SCI-1D | 10 | 2 |
| 14 | 2.5 | SCI-2D | 8 | 1 |
| 15 | 2.5 | SSI-1D | 6 | 4 |
| 16 | 2.5 | SSI-2D | 4 | 3 |
| 17 | 3 | SCI-1D | 4 | 1 |
| 18 | 3 | SCI-2D | 6 | 2 |
| 19 | 3 | SSI-1D | 8 | 3 |
| 20 | 3 | SSI-2D | 10 | 4 |
| 21 | 3.5 | SCI-1D | 6 | 3 |
| 22 | 3.5 | SCI-2D | 4 | 4 |
| 23 | 3.5 | SSI-1D | 10 | 1 |
| 24 | 3.5 | SSI-2D | 8 | 2 |
| 25 | 4 | SCI-1D | 8 | 4 |
| 26 | 4 | SCI-2D | 10 | 3 |
| 27 | 4 | SSI-1D | 4 | 2 |
| 28 | 4 | SSI-2D | 6 | 1 |
| 29 | 4.5 | SCI-1D | 10 | 2 |
| 30 | 4.5 | SCI-2D | 8 | 1 |
| 31 | 4.5 | SSI-1D | 6 | 4 |
| 32 | 4.5 | SSI-2D | 4 | 3 |
| 33 | 5 | SCI-1D | 4 | 1 |
| 34 | 5 | SCI-2D | 6 | 2 |
| 35 | 5 | SSI-1D | 8 | 3 |
| 36 | 5 | SSI-2D | 10 | 4 |
| 37 | 5.5 | SCI-1D | 6 | 3 |
| 38 | 5.5 | SCI-2D | 4 | 4 |
| 39 | 5.5 | SSI-1D | 10 | 1 |
| 40 | 5.5 | SSI-2D | 8 | 2 |
| 41 | 6 | SCI-1D | 8 | 4 |
| 42 | 6 | SCI-2D | 10 | 3 |
| 43 | 6 | SSI-1D | 4 | 2 |
| 44 | 6 | SSI-2D | 6 | 1 |
| 45 | 6.5 | SCI-1D | 10 | 2 |
| 46 | 6.5 | SCI-2D | 8 | 1 |
| 47 | 6.5 | SSI-1D | 6 | 4 |
| 48 | 6.5 | SSI-2D | 4 | 3 |

**Simulated Annealing**

Simulated annealing is a metaheuristic technique developed in the early 1980s that mathematically mirrors the cooling of a material to a state of minimum energy.[25] If a material cools too quickly, the crystals within the material will harden in a suboptimal configuration. Likewise, the premise behind the simulated annealing algorithm is the assertion that if a solution is converged on too quickly, that solution will be suboptimal. Simulated annealing was chosen over the other two well-known metaheuristics of genetic algorithms and the tabu search because of its relative ease of implementation, lower computational requirements, and better success rate in finding the optimal solution to similar complex problems.[26]

First, the objective function, or system energy $E(\Gamma)$, to be minimized by the algorithm must be defined:

$$E(\Gamma) = f(\gamma_1 \quad \gamma_2 \quad \cdots \quad \gamma_n) \tag{15}$$

Each $\gamma$ represents a different DSS architecture variable, such as the orbital altitude or total number of satellites. The algorithm begins with an initial state vector $\Gamma_i$ containing randomly chosen values for each design vector variable within the bounds placed on that variable. The value of the objective function $E(\Gamma_i)$ is then computed for this design vector. Next, the design vector is randomly perturbed to find a new design vector ($\Gamma_{i+1}$) in the neighborhood (a neighbor is a design vector that has all but one identical entries as the original design vector) of the current design vector, and the new $E(\Gamma_{i+1})$ is computed. If $E(\Gamma_{i+1}) < E(\Gamma_i)$, then $\Gamma_{i+1}$ is accepted as the new design vector. If $E(\Gamma_{i+1}) > E(\Gamma_i)$, $\Gamma_{i+1}$ can still be accepted as the new design vector with a probability

$$\text{Prob}(E) = e^{(-\Delta/T)} \tag{16}$$

where

$$\Delta = E(\Gamma_{i+1}) - E(\Gamma_i) \tag{17}$$

$T$ is the system temperature, a parameter that decreases as the number of iterations in the optimization increases. Thus the likelihood of accepting a design vector with a greater system energy decreases over time. The ability to accept a less optimal $\Gamma_{i+1}$ reduces the chance that the algorithm's solution will become trapped in a local minimum. This procedure is repeated until no new solutions are accepted after a specified number of iterations. In theory, the algorithm converges to the optimal solution as the system temperature lowers toward zero. Unlike linear or integer programming methods, however, metaheuristic solutions are not guaranteed to be global optima.

For the TPF case study, the four elements of the design vector in Eq. (15) are 1) heliocentric orbital altitude, 2) architecture (SSI vs SCI, 1D vs 2D), 3) number of collector apertures, and 4) collector aperture diameter. CPI replaces system energy as the metric to be minimized. The initial system temperature $T_i$ was set to 1000 and was multiplied by a factor of 0.85 after each iteration. The algorithm was terminated after the completion of 48 iterations.

**Pseudogradient Search**

The French mathematician Pierre Fermat introduced some of the first formal ideas in the field of optimization, including the observation that at the maximum and the minimum of a function the tangent line of any curve would be horizontal. Fermat's observation was implemented mathematically to find maxima and minima through the derivative operation. Even functions with multiple variables could now be optimized through the use of partial derivatives.

Unfortunately, DSS design problems are discreet rather than continuous. This lack of continuity violates calculus' extreme value theorem and thus prevents the use of derivatives to find designs that maximize or minimize the metric of choice.

Finite differencing, however, may be used to approximate the sensitivity of a particular point design to a change in each element of the design vector:

$$\delta = f(\Gamma_{i+1}) - f(\Gamma_i) \tag{18}$$

where $\delta$ is the difference in the metric of choice resulting from a unit change in one element of the design vector $\Gamma$. The gradient $\nabla$ with respect to that element of the design vector is then

$$\nabla = \delta/(\gamma_{i+1} - \gamma_i) \tag{19}$$

where $\gamma$ is the element of the design vector that was perturbed. Depending on the slope of the gradient, a new design vector may be defined by moving the variable about which the gradient was computed in the direction that either increases or decreases the design metric, depending on whether the goal of the problem is maximization or minimization. This modified version of the gradient search works on the assumption that the output metric is approximated to be piecewise linear when only a single element of the design vector changes. Because the design problem is not convex in general, however, this algorithm may get trapped in a local extrema.

For the TPF case study, an initial design vector was chosen by a random-number generator. One then computes the gradient of the CPI metric about the heliocentric orbital altitude, number of apertures, and aperture diameter elements of the design vector by changing each of these elements by one unit and then performing the finite-differencing calculation. For the architecture element of the design vector, one computes the gradient of the CPI metric by performing a finite difference for all three remaining architectures. One then selects a new design vector by perturbing each element of the design vector one unit in the direction with the largest negative CPI

gradient. Thus one run of the gradient search requires the evaluation of seven separate TPF architectures—six for finite differencing and one to evaluate the new design vector. For the TPF case study, this algorithm was applied seven successive times, starting from the randomly generated initial design vector, resulting in the evaluation of 50 design vectors before arriving at the "best" solution. Because the generation of the initial design vector is a stochastic process, the gradient search algorithm was applied 10 times with 10 different randomly generated initial design vectors.

#### Single-Variable-Axis Exploration

The final optimization method explored for DSS design is not a true optimization technique, but is a common practice for initially exploring the trade space of a complex problem. First, a baseline design vector is chosen. Next, a single element $\gamma_i$ of the design vector $\Gamma$ is varied over its entire allowable range, while all of the remaining design vector elements are held constant at their baseline values. If the goal is objective function minimization, the new value for $\gamma_i$ in the new design vector $\Gamma_{i+1}$ is the value that produced the minimum objective value over the examined range. This process is repeated for each element of the design vector, with the other nonvarying $\gamma_i$ maintaining their original baseline values until every element in the design vector has been plotted over its allowable range. The new design vector $\Gamma_{i+1}$ is then created by taking the value of each $\gamma_i$ that minimized the objective function. If desired, $\Gamma_{i+1}$ may be used as a new baseline design vector about which to repeat this process of exploring each axis individually.

This algorithm has many potential drawbacks. First, it is computationally expensive as every value of each element of the design vector must be tested before a new solution is converged on. Second, this approach fails to capture the coupled effects that combinations of design vector elements can have on the objective function. Finally, the final solution depends on the initial baseline design vector, and the final solution is not necessarily the global optimum. Nevertheless, the approach should work fairly well for DSSs with shallow trade spaces. Additionally, the single-variable-axis algorithm provides the benefit of giving the designer a feel for the system trade space—such as how the performance of a system varies as the orbit varies, all other things held constant. Neither the simulated annealing nor the gradient search algorithms provide this additional benefit, giving only a single final solution.

For the TPF case study, the baseline design vector was chosen by a random-number generator. The single-variable-axis exploration algorithm was then executed over two successive runs, with each run requiring the evaluation of 22 separate design vectors, to converge on a final solution. Because the generation of the initial baseline design vector is a stochastic process, this algorithm was applied 10 times with 10 different randomly generated initial baseline design vectors.

## Results

After each of the four MDO techniques has been applied to the TPF design problem, their performance at finding good solutions after evaluating less than 8% of the total system trade space may be analyzed. Both the Taguchi analysis and the simulated annealing algorithm evaluated 48 TPF design vectors to arrive at a solution. The pseudogradient search and single-axis exploration techniques evaluated 50 and 47 design vectors, respectively, before converging on a solution. Unfortunately, it was not possible to have all four MDO methods evaluate an identical number of design vectors before solution convergence because the pseudogradient search and single-axis exploration techniques converge on a new solution after the evaluation of every 7 and 22 design vectors, respectively. However, a solid comparison among the effectiveness of all four MDO methods may still be made as the numbers of design vector evaluations for solution convergence are within 0.5% of each other—the single-axis technique tests 7.3% of the 640 possible TPF architectures at the low extreme and the pseudogradient technique searches 7.8% of the TPF architectures at the high extreme.

To determine the accuracy of these four MDO methods, the CPI was computed for all 640 full-factorial TPF design vectors. When the best solution from each MDO method is compared with the true optimal solution found by complete enumeration, the performance of each MDO technique can be quantitatively assessed. Although complete enumeration to find the true optimal solution was possible for this controlled experiment, an expansion of the design vector $\Gamma$, both by including more independent variables $\gamma_i$ and considering more possible values for each independent variable, could quickly make full enumeration of potential design vectors a computationally impractical approach. Rather, the results of this work should identify which MDO techniques can quickly find good solutions by evaluating a minimum number of alternative design vectors for large, complex DSS design problems.

From complete enumeration of all 640 possible design vectors, the true optimal solution to the design problem was found to be an architecture with a structurally connected two-dimensional configuration located at 4 AU, with eight collector apertures, each of which is 4 m in diameter. This TPF architecture minimized the CPI metric at a value of $469.6 thousand per image.

The mean CPI for the 48 TPF design vectors evaluated in the Taguchi analysis matrix of Table 2 was $818.2 thousand. After each CPI was converted to a SNR, the balanced mean was computed from Eq. (12) to be −57.8 dB. The optimized TPF design architecture is determined by setting each of the four design vector variables to the value that yields the largest SNR (shown in boldface type in Table 3). In this manner, Taguchi's method converges on a structurally connected two-dimensional interferometer located at 3 AU with six collector apertures, each 4 m in diameter, as the best design.

Tables 3 and 4 illustrate the results from the Taguchi analysis. With Eq. (14), the predicted CPI of this architecture is found to be $465.1 thousand. The actual performance of this architecture was evaluated when the Taguchi predicted best TPF design vector was entered into the TMAS, which computed the true CPI as $499.1 thousand. Thus the CPI of the Taguchi predicted best architecture differs from the true optimal architecture by 6.1%. Inspection of the design vectors reveals that Taguchi's method did converge on the correct optimal values for the collector connectivity/geometry and aperture diameter, but failed to select the optimal orbit and number of collector apertures.

In addition to searching for the optimal solution, Taguchi's method may also be used to determine the relative importance of each element of the design vector through an analysis of variance (ANOVA). ANOVA is a statistically based tool for detecting

**Table 3 Taguchi analysis results**

| Orbit, AU | SNR | Collector connectivity/ geometry | SNR | Number of collector apertures | SNR | Collector diameter, m | SNR |
|---|---|---|---|---|---|---|---|
| 1.0 | −60.7 | SCI | | 4 | −59.9 | 1 | −60.8 |
| 1.5 | −57.4 | 1D | −57.6 | 6 | **−57.0** | 2 | −58.0 |
| 2.0 | −57.8 | **2D** | −57.1 | 8 | −57.2 | 3 | −56.7 |
| 2.5 | −57.9 | | | 10 | −57.1 | **4** | **−55.7** |
| **3.0** | **−57.0** | SSI | | | | | |
| 3.5 | −57.1 | 1D | −57.9 | | | | |
| 4.0 | −57.2 | 2D | −58.6 | | | | |
| 4.5 | −58.3 | | | | | | |
| 5.0 | −57.4 | | | | | | |
| 5.5 | −57.3 | | | | | | |
| 6.0 | −57.4 | | | | | | |
| 6.5 | −58.5 | | | | | | |

**Table 4 Optimized configuration from Taguchi analysis**

| Description | Value |
|---|---|
| Taguchi predicted optimum architecture | 3 AU, SCI-2D, 6 apertures, 4 m |
| Taguchi predicted optimum architecture CPI ($k) | 465.1 |
| Actual CPI ($k) of Taguchi predicted optimum | 499.1 |
| Taguchi error from predicted optimum | 7.1% |
| True optimum architecture | 4 AU, SCI-2D, 8 apertures, 4 m |
| True optimum CPI ($k) | 469.6 |
| Taguchi error from true optimum | 6.1% |

differences in the average performance of groups of items tested.[24] First, a parameter named the sum of squares (Σ Sq) is computed:

$$\Sigma\,\mathrm{Sq}_\gamma = \sum_{i=1}^{n} n_{\gamma_i}\left(m_{\gamma_i} - m\right)^2 \tag{20}$$

where $n$ is the number of potential different values for design vector variable $\gamma$, $n_{\gamma_i}$ is the number of rows in the orthogonal test matrix with design vector variable $\gamma$ at setting $i$, $m_{\gamma_i}$ is the main effect of design vector variable $\gamma$ at setting $i$ from Eq. (13), and $m$ is the balanced mean from Eq. (12). The relative influence RI can then be computed with knowledge of the error variance $v_e$ and the degrees of freedom (DOF) of design variable $\gamma_x$:

$$\mathrm{RI} = \frac{\Sigma\,\mathrm{Sq}_{\gamma_i} - (v_e)(\mathrm{DOF}_{\gamma_i})}{\sum_{i=1}^{n_{\gamma x}} \Sigma\,\mathrm{Sq}_i} \tag{21}$$

Table 5 shows that, of the four parameters in the TPF design vector, the aperture diameter exerts by far the greatest relative influence on the CPI. Thus, although Taguchi's method failed to find the true optimal solution, it still provided useful information to the designer concerning the relative effect each element of the design vector has on the CPI metric.

Because the three remaining MDO techniques may vary as a function of their starting point, are probabilistic in nature, and can converge on a local minima, 10 trials were executed for each technique. Each trial began with a different, randomly generated initial design vector. Table 6 illustrates the results of each trial for each algorithm.

Both the gradient search and single-axis exploration algorithms converged on the true optimal solution 4 out of 10 times. However, in instances in which the true optimal solution is unknown, how can the confidence in the results of MDO techniques that incorporate randomness be ascertained? It turns out that confidence estimates may be made by exercising the theory of continuous probability distributions.

Table 6 also lists the mean $\mu$ (in this case $\mathrm{CPI}_{\mathrm{avg}}$), standard deviation $\sigma$, and variance $v$ associated with the results from each MDO technique. These values characterize the distribution for each set of results. The normal distribution density function

$$f(x) = \left(1/\sqrt{2\pi\sigma}\right)\exp\left\{-\left(\tfrac{1}{2}\right)[(x-\mu)/\sigma]^2\right\}, \qquad -\infty < x < \infty \tag{22}$$

can be used to solve many problems in science and engineering. By binning the 640 TPF CPI's into $k$ cells and comparing the observed density $o_i$ in each cell $i$ with the expected density $e_i$ in each cell $i$, the chi-squared ($\chi^2$) test

$$\chi^2 = \sum_{i=1}^{k} \frac{(o_i - e_i)^2}{e_i} \tag{23}$$

may be applied to statistically determine whether the full-factorial trade space follows a standard normal distribution. The chi-squared test showed that the standard normal distribution failed the null hypothesis. Rather, the TPF trade space CPI data follow a gamma distribution:

$$f(x) = \begin{cases} [1/\beta^\alpha \Gamma(\alpha)]x^{\alpha-1}e^{-x/\beta}, & x > 0 \\ 0, & \text{elsewhere} \end{cases} \tag{24}$$

where

$$\Gamma(\alpha) = (\alpha-1)!, \qquad \alpha = \mu^2/\sigma^2, \qquad \beta = \mu \big/ \sqrt{\alpha} \tag{25}$$

Figure 6 illustrates the gamma distribution for the TPF trade space. This distribution exhibits an $\alpha$ value of 5.37 and a $\beta$ value of 154. A measure of the degree of confidence CI in the best found solution may then be made by finding the area under the gamma distribution curve to the right of the best solution found, illustrated by the shaded region in Fig. 6:

$$\mathrm{CI} = \int_{\mathrm{CPI}_{\mathrm{min}}}^{\infty} \frac{1}{\beta^\alpha \Gamma(\alpha)} x^{\alpha-1}e^{-x/\beta}\,\mathrm{d}x \tag{26}$$

CI provides a quantitative metric of the confidence that the solution found by a MDO technique, after a given number of trials, is indeed the true optimal solution independent of the knowledge of the full-factorial trade space. According to this metric, the solutions obtained by the simulated annealing and single-axis exploration algorithms are more likely to be correct than the solutions found by a gradient search, which appears to be more susceptible to getting stuck in a local minima than the other two methods.

**Table 5 Taguchi ANOVA**

| Parameter | Σ Squares, $\mathrm{dB}^2$ | Degrees of freedom | Variance, $\mathrm{dB}^2$ | Relative influence, % |
|---|---|---|---|---|
| Orbit | 44.8 | 11 | 4.1 | 11.4 |
| Aperture connectivity/ geometry | 13.2 | 3 | 4.4 | 3.4 |
| Number of apertures | 72.3 | 3 | 24.1 | 21.4 |
| Aperture diameter | 179.5 | 3 | 59.8 | 54.1 |
| Error | 18.2 | 27 | 0.7 | 9.7 |
| Total | 328.0 | 47 | | 100.0 |

**Table 6 Simulated annealing, gradient search, and single-axis algorithm results**

| Parameter | Simulated annealing | Pseudogradient search | Single axis |
|---|---|---|---|
| Trial | CPI ($k) | CPI ($k) | CPI ($k) |
| 1 | 493.8 | 470.8 | 469.6 |
| 2 | 470.0 | 470.0 | 469.6 |
| 3 | 469.6 | 469.6 | 513.8 |
| 4 | 505.1 | 520.9 | 469.6 |
| 5 | 470.8 | 469.6 | 526.0 |
| 6 | 470.8 | 469.6 | 513.8 |
| 7 | 493.8 | 532.6 | 470.8 |
| 8 | 470.0 | 469.6 | 525.9 |
| 9 | 498.2 | 470.8 | 469.6 |
| 10 | 496.4 | 483.0 | 473.9 |
| $\mathrm{CPI}_{\mathrm{avg}}$ | 483.9 | 482.7 | 490.3 |
| $\sigma$ | 14.7 | 23.8 | 25.8 |
| $v$ | 215.6 | 564.5 | 667.7 |
| $\alpha$ | 1083 | 411 | 361 |
| $\beta$ | 0.447 | 1.17 | 1.36 |
| CI | 84% | 68% | 79% |

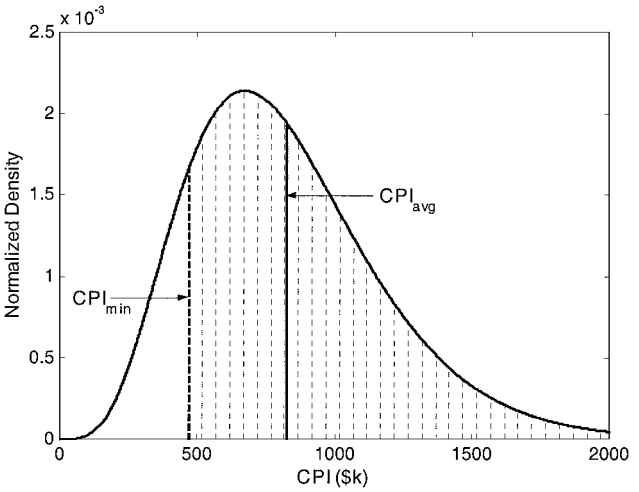


**Fig. 6 Gamma distribution for the TPF full-factorial trade space.**

## Analysis of Results

Three out of the four investigated MDO techniques—simulated annealing, pseudogradient search, and single-axis exploration—found the true optimal solution for the TPF design problem. The remaining technique, Taguchi analysis, converged on a solution with a CPI 6.1% worse than the optimal solution. The plot on the left in Fig. 7 illustrates the full-factorial trade space for the TPF design

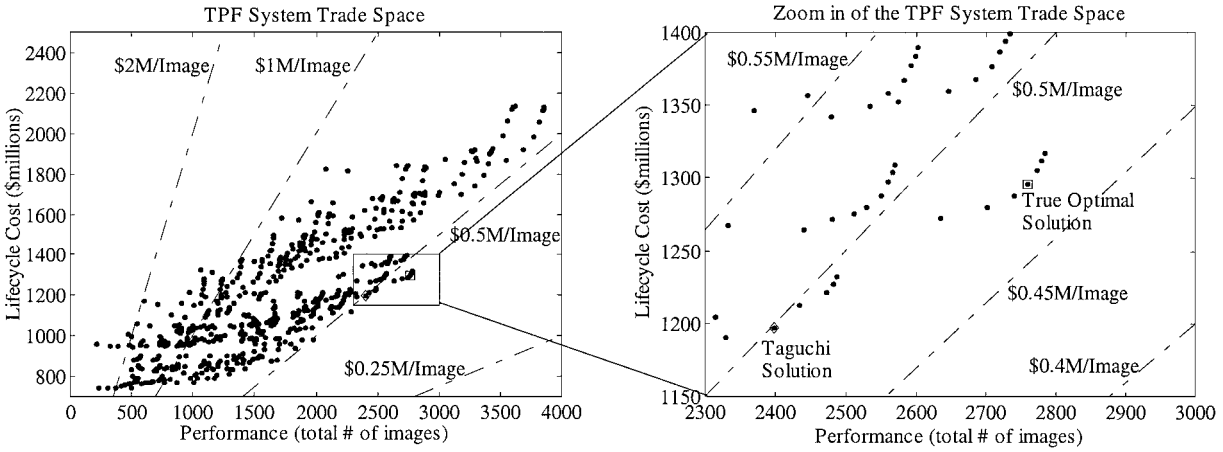


**Fig. 7 TPF full-factorial trade space with the true and Taguchi optimal solutions.**

case study along with lines of constant CPI. The line connecting the points closest to the lower-right-hand corner of this plot defines the Pareto-optimal front of the TPF trade space. Pareto optimization embodies the principle of optimizing multiple competing objectives—in this case, minimizing total lifecycle cost while simultaneously maximizing total system performance (measured as the total number of "images" produced). Along this Pareto-optimal front, a design vector cannot be chosen to improve performance without also increasing life-cycle cost and vice versa.

The zoom-in plot on the right shows the location of the true and Taguchi optimal solutions in the system trade space. Note that all four techniques were able to find the region in the trade space with the best solutions on the basis of the CPI metric after evaluating less than 8% of the total trade space. Although complete enumeration guarantees optimality and was possible in this case, the exponential growth rate in the number of design options as a function of the design vector size makes an exhaustive search impractical for large problems. These results illustrate how MDO methods may be successfully applied to large problems to find good design solutions efficiently during the conceptual design of a DSS.

If this case study design were being carried out to the next stage, all of the design architectures in the local family of solutions comprising the arc in which the true optimal solution lies merit further detailed analysis as the difference between their CPIs is within the uncertainty of the computations. Figure 8 illustrates this arc. The performance of all these mission architectures lies within 150 images of each other, and total life-cycle cost varies by only $45M. Note that three of the four design vector elements remain constant through the arc—collector connectivity/geometry (structurally connected, two dimensional), number of apertures (eight), and aperture diameter (4 m). The only design vector parameter that varies through the arc is the heliocentric orbital altitude, with the true optimal solution occurring at 4 AU. Based on these results, the family of solutions defined by this arc merits further detailed study in the next mission design phase. This example illustrates how the application of MDO techniques can help focus the design effort during the conceptual design phase of a program.

Taguchi's method was the only MDO technique tested that failed to find the true optimal solution. Additionally, the use of precise orthogonal arrays in Taguchi's method tends to force the design vector to be tailored to the test matrix. In other words, the solution technique drives the formulation of the problem rather than vice versa. For example, in the TPF test study the heliocentric orbital altitudes of 6.0 and 6.5 AU, which were not in the system trade space, were required to create a valid orthogonal test matrix. Increasing the number of variables and potential variable values in the design vector will only make the formulation of an orthogonal test matrix more difficult, and may even become prohibitive for systems with larger, more complex trade spaces. From the results of this work, Taguchi's method does not appear to be the best MDO approach for the design of distributed satellite systems with deep trade spaces. However, the ANOVA applied to the Taguchi results did provide valuable design

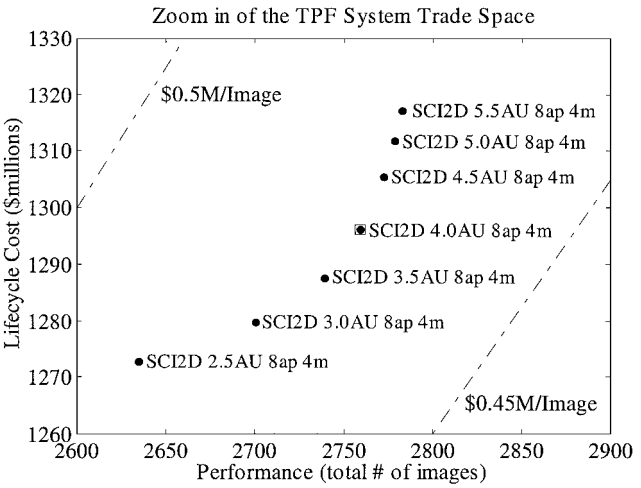


**Fig. 8 Optimal arc family.**

information, and attempts should be made to apply similar ANOVA tools to the analysis of data from the other MDO techniques.

The metaheuristic simulated annealing algorithm found the best solution only once, but consistently found good solutions with a greater degree of confidence than any of the other MDO techniques. This result is evidenced by the fact that the simulated annealing algorithm recorded the highest CI of 84%. This strong showing of simulated annealing is consistent with the application of simulated annealing to other difficult problems[26] and is most likely a result of the algorithm's ability to escape local minima by sometimes allowing random moves to neighboring solutions worse than the current solution. A local minima is a design vector that has a lower CPI than any neighboring design vector, but does not have the lowest CPI in the entire system trade space. As more complex DSSs with larger design vectors are likely to contain many local minima throughout the trade space, simulated annealing appears to be a good MDO technique to apply to future DSS designs and should be investigated further on more complex problems. Furthermore, the success of the heuristic simulated annealing algorithm warrants future consideration of the other two metaheuristics, genetic algorithms and tabu search, as well.

Of the four MDO methods explored, the pseudogradient search was the most likely to converge on a local minima. This entrapment in local minima occurs because the pseudogradient search algorithm has no way to extricate itself when all of the investigated local gradients are positive. When this situation occurs, the algorithm believes it has found the optimal solution and becomes permanently stuck in the local minima. The fact that the pseudogradient search found the true optimal solution 4 of 10 times for TPF can be attributed to the fact that the case study contained a relatively shallow trade space with only 640 possible solutions. From these results, the pseudogradient

search algorithm that uses a modified finite-differencing approach does not appear to be a promising technique for the design of future DSSs with deep trade spaces.

The final MDO approach tested, the single-axis exploration algorithm, also converged on the true optimal solution 4 of 10 times, but did so with a degree of confidence much greater than that of the pseudogradient search and only slightly less than the simulated annealing algorithm. Unlike the pseudogradient search approach, the single-axis exploration algorithm explores every possible neighbor before moving to a new solution. Although the single-axis exploration algorithm still fails to capture the coupling between design vector parameters, it is less likely to get, but is not immune to getting, stuck in local minima. The strong showing in the TPF test case of this MDO approach, combined with the additional information the single-axis exploration algorithm provides concerning the relationship between design vector parameters and output metrics, merits the further study of the single-axis exploration algorithm for DSS design.

It should be stressed that these results are particular to the TPF case study. The trade space for this case study was relatively shallow to allow for complete enumeration in order to determine the true global optimum as a reference point. The relative performance of the four MDO approaches applied to the TPF may differ as the size and the depth of the trade space increase. Determining how the performance of these algorithms scales with problem complexity and trade space depth is a subject of ongoing research.

## Conclusions

The application of four separate MDO techniques to the design of complex, highly coupled DSSs has been demonstrated. In particular, the simulated annealing and single-axis exploration algorithms efficiently found good conceptual design solutions with a high degree of confidence after evaluating less than 8% of the entire full-factorial TPF trade space, which contained 640 separate unique design architectures. These two methods merit further study for application to the design of other DSSs with larger design vectors and deeper trade spaces. For the TPF case study, a structurally connected two-dimensional array architecture located at 4 AU with eight collector apertures, each 4 m in diameter, was found to minimize the CPI metric at $469.6 thousand. The full-factorial data were used to verify the performance of the MDO techniques.

Merely finding point designs, however, does not satisfy system engineers during the conceptual design stage of a project. Additional information on the relationships between the system parameters and the system metrics is desired in the conceptual design phase when requirements and constraints may be ill defined or may change frequently. The analysis of variance tools applied under Taguchi's method yielded insight to the relative effect each element of the design vector exerted on the CPI metric for TPF. Other tools, specifically sensitivity analysis tools, must be explored and developed to provide more information characterizing the trade space about a particular solution. Such sensitivity tools will increase the credibility and the utility of the DSS design solutions provided by MDO techniques for the space systems engineering community. In short, MDO methods incorporating life-cycle cost models with sensitivity analysis tools hold the potential to improve greatly the conceptual design of DSSs by efficiently exploring the system trade space of highly coupled problems to find potential design architecture solutions that might not otherwise be considered.

## Acknowledgments

The authors thank the members of the Massachusetts Institute of Technology Spring-99 16.89 class for creating and documenting the TMAS software. The authors also thank Edmund Kong for his insight and feedback and Olivier de Weck for creating the finite element model illustrated in Fig. 5.

## References

[1]Subramanian, J., Stidham, S., and Lautenbacher, C. J., "Airline Yield Management with Overbooking, Cancellations, and No-Shows," *Transportation Science*, Vol. 33, May 1999, pp. 147–167.

[2]Mathaisel, D. F. X., "Decision Support for Airline Schedule Planning," *Journal of Combinatorial Optimization*, Vol. 1, No. 3, 1997, pp. 251–275.

[3]Stettner, L., "Risk Sensitive Portfolio Optimization," *Mathematical Methods of Operations Research*, Vol. 50, No. 3, 1999, pp. 463–474.

[4]Mosher, T., "Applicability of Selected Multidisciplinary Design Optimization Methods to Conceptual Spacecraft Design," *Proceedings of the 6th AIAA/NASA/ISSMO Symposium on Multidisciplinary Analysis and Optimization*, AIAA, Reston, VA, 1996, pp. 664–671.

[5]Riddle, E., "Use of Optimization Methods in Small Satellite Systems Analysis," *Proceedings of the 12th AIAA/USU Conference on Small Satellites*, Paper SSC98-X-1, Utah State Univ., Logan, UT, Sept. 1998.

[6]Shishko, R., and Chamberlain, R., *NASA Systems Engineering Handbook*, SP-6105, NASA, June 1995, pp. 17, 77–82.

[7]Shaw, G. B., Miller, D. W., and Hastings, D. E., "Generalized Characteristics of Communication, Sensing, and Navigation Satellite Systems," *Journal of Spacecraft and Rockets* (to be published).

[8]Sobieszczanski-Sobieski, J., "Multidisciplinary Design Optimization: An Emerging New Engineering Discipline," *Proceedings of the World Congress on Optimal Design of Structural Systems*, 1993.

[9]Mosher, T., "Spacecraft Design Using a Genetic Algorithm Optimization Approach," *Proceedings of the 1998 IEEE Aerospace Conference*, Vol. 3, Inst. of Electrical and Electronics Engineers, New York, 1998, pp. 123–134.

[10]Matossian, M. G., "Earth Observing System Constellation Design Through Mixed Integer Programming," *Space Technology*, Vol. 16, No. 5/6, 1996, pp. 233–243.

[11]Matthews, C., *Case Studies in Engineering Design*, Arnold Publishers, London, 1998.

[12]Beichman, C. A., "The Terrestrial Planet Finder: The Search for Life-Bearing Planets Around Other Stars, *Proceedings of the SPIE Conference on Astronomical Interferometry*, SPIE 3350, Pt. 2, Society of Photo-Optical Instrumentation Engineers, Bellingham, WA, 1998, pp. 719–723.

[13]Beichman, C. A., Woolf, N. J., and Lindensmith, C. A., "The Terrestrial Planet Finder (TPF): A NASA Origins Program to Search for Habitable Planets," JPL Pub. 99-3, May 1999, pp. 49–55, 87–89.

[14]Wong, R., "Cost Modeling," *Space Mission Analysis and Design*, 2nd ed., edited by W. J. Larson and J. R. Wertz, Microcosm, Torrance, CA, 1992, pp. 715–740.

[15]Isakowitz, S. J., *International Reference Guide to Space Launch Systems*, 2nd ed., AIAA, Washington, DC, 1995.

[16]Curtis, A., deWeck, O., Frazzoli, E., Girerd, A., Hacker, T., Jilla, C., Kong, E., Makins, B., Pak, S., and Miller, D., "ASTRO—Architecting the Search for Terrestrial planets and Related Origins," Massachusetts Inst. of Technology Space Systems Lab., SERC 6-99, Cambridge, MA, June 1999, pp. 115–141.

[17]Jilla, C. D., and Miller, D. W., "A Reliability Model for the Design and Optimization of Separated Spacecraft Interferometer Arrays," *Proceedings of the 11th AIAA/USU Conference on Small Satellites*, Paper SSC97-XI-2, Utah State Univ., Logan, UT, Sept. 1997.

[18]Gelb, A., ed., *Applied Optimal Estimation*, MIT Press, Cambridge, MA, 1974, pp. 42–45.

[19]Miller, D. W., Curtis, A., de Weck, O., Frazzoli, E., Girerd, A., Hacker, T., Jilla, C. D., Kong, E. M., Makins, B., and Pak, S., "Architecting the Search for Terrestrial Planets and Related Origins (ASTRO)," *Airborne and Space Telescopes and Astronomical Instrumentation*, Vol. 4013, Society of Photo-Optical Instrumentation of Engineers, Bellingham, WA (to be published).

[20]Shaw, G. B., Miller, D. W., and Hastings, D. E., "Development of the Quantitative Generalized Information Network Analysis Methodology for Satellite Systems," *Journal of Spacecraft and Rockets* (to be published).

[21]Logothetis, N., and Wynn, H. P., *Quality Through Design: Experimental Design, Off-Line Quality Control, and Taguchi's Contributions*, Clarendon, Oxford, 1989, pp. 1–20.

[22]*Glossary and Tables for Statistical Quality Control*, 2nd ed., American Society for Quality Control, Milwaukee, WI, 1983, pp. 85, 86.

[23]Wu, K. C., and Lake, M. S., "Multicriterion Preliminary Design of a Tetrahedral Truss Platform," *Journal of Spacecraft and Rockets*, Vol. 33, No. 3, 1996, pp. 410–415.

[24]Ross, P. J., *Taguchi Techniques for Quality Engineering: Loss Function, Orthogonal Experiments, Parameter and Tolerance Design*, 2nd ed., McGraw–Hill, New York, 1996, pp. 208–212.

[25]Kirkpatrick, S., Gelatt, C. D., and Vecchi, M. P., "Optimization by Simulated Annealing," *Science*, Vol. 220, No. 4598, 1983, pp. 671–680.

[26]Brooks, R. R., Iyenger, S. S., and Rai, S., "Comparison of Genetic Algorithms and Simulated Annealing for Cost Minimization in a Multisensor System," *Optical Engineering*, Vol. 37, No. 2, 1998, pp. 505–516.

A. C. Tribble
*Associate Editor*